Resource allocation accounts for the large variability of rate-yield phenotypes across bacterial strains

Valentina Baldazzi,[1,2,*] Delphine Ropers,[3] Jean-Luc Gouzé,[1]
Tomas Gedeon,[4] Hidde de Jong[3,*]

[1]Université Côte d'Azur, Inria, INRAE, CNRS, UPMC Univ Paris 06,
06902 Sophia Antipolis, France
[2]INRAE, Institut Sophia-Agrobiotech, 06903 Sophia Antipolis, France
[3]Université Grenoble Alpes, Inria, 38000 Grenoble, France
[4]Montana State University, Bozeman, MT 59717, USA

*Corresponding authors: valentina.baldazzi@inria.fr, hidde.de-jong@inria.fr

April 27, 2022

Abstract

Different strains of a microorganism growing in the same environment display a wide variety of growth rates and growth yields. We developed a coarse-grained model to test the hypothesis that different resource allocation strategies, corresponding to different compositions of the proteome, can account for the observed rate-yield variability. The model predictions were verified by means of a database of hundreds of published rate-yield and flux phenotypes of *Escherichia coli* strains grown in standard laboratory conditions. We found a very good quantitative agreement between the predicted and observed variability in rates and yields. Moreover, over the entire range of wild-type and mutant strains considered, acetate overflow was predicted not to correlate with the growth rate, in agreement with the experimental data. These results support the hypothesis that resource allocation is a major explanatory factor of the observed variety of growth rates and growth yields across different bacterial strains. We also show, however, that differences in enzyme activity need to be taken into account to explain variations in protein abundance. Our model allows a fundamental understanding of quantitative bounds on rate and yield in *E. coli* and other microorganisms. It may also be useful for the rapid screening of strains in metabolic engineering and synthetic biology.

Introduction

Microbial growth consists of the conversion of nutrients from the environment into biomass. This flux of material is coupled with a flux of energy from the substrate to small energy cofactors (ATP, NADH, NADPH, ...) driving biomass synthesis forward and releasing energy in the process [1]. The growth of microorganisms has been profitably analyzed from the perspective of resource allocation, that is, the assignment of limiting cellular resources to the different

biochemical processes underlying growth [2, 3, 4, 5, 6, 7, 8, 9, 10, 11, 12]. It is often considered that proteins, the main component of biomass, are also the bottleneck resource for growth. Proteins function as enzymes in carbon and energy metabolism and they constitute the molecular machines responsible for the synthesis of macromolecules, in particular proteins themselves. The composition of the proteome in a given growth condition can therefore be interpreted as the resource allocation strategy adopted by the cells to exploit available nutrients.

Two macroscopic criteria for characterizing microbial growth are growth rate and growth yield. The former refers to the rate of conversion of substrate into biomass, and the latter to the efficiency of the process, that is, the fraction of substrate converted into biomass. Several empirical relations between proteome composition *vs* growth rate and growth yield have been established. A linear relation between growth rate and the ribosomal protein fraction of the proteome holds over a large range of growth rates and for a variety of microbial species [2, 13, 14]. Variants of this so-called growth law have been found for cases of reduced translation capacities [2] or different temperatures [15, 16]. While the ribosomal protein fraction increases with the growth rate, the proteome fraction allocated to energy metabolism decreases [17, 18]. Moreover, within this decreasing fraction, *Escherichia coli* and other microorganisms move resources from respiration to fermentation pathways [17]. Simple mathematical models have been proposed to account for the above relations in terms of the requirements of self-replication of the proteome and the relative protein costs and ATP yields of respiration and fermentation [2, 4, 5, 6, 8, 11, 16, 17, 19].

Most of these relations have been studied in experiments in which the same strain exhibits a range of growth rates in different environments, with different carbon sources. Even for a fixed environment, however, different strains of the same species may grow at very different rates and yields. For example, in a comparative study of seven *E. coli* strains, growth rates ranging from 0.61 to 0.97 h^{-1}, and (carbon) growth yields between 0.52 and 0.66, were observed during aerobic growth on glucose [20]. Since the genes encoding enzymes in central carbon and energy metabolism are largely shared across the strains [20], the yield differences are not due to different metabolic capacities but rather to different regulatory strategies, that is, different usages of the metabolic pathways of the cell. As another example, evolution experiments with *E. coli* have given rise to evolved strains that grow more than 40% faster, sometimes with higher growth yields, than the ancestor strain in the same environment [21]. Analysis of the underlying mutations reveals that the higher rates and yields of the evolved strains are not due to new metabolic capacities, but rather to modified regulatory strategies [21, 22].

Can the large variability of rate-yield phenotypes observed across different strains of the same species be explained by different resource allocation strategies, that is, different compositions of the proteome? In order to answer this question, we developed a coarse-grained resource allocation model that couples the fluxes of carbon and energy underlying microbial growth. The model was calibrated by means of existing data in the literature, without any parameter fitting, and its predictions were compared with a database of several hundreds of pairs of rates and yields of *E. coli* strains reported in the literature. The database includes wild-type strains as well as mutant strains obtained through directed mutagenesis or adaptive laboratory evolution (ALE).

We found that the predicted rates and yields in different growth conditions correspond very well with the observed variability of rate-yield phenotypes. The model also accounts for

the associated substrate uptake and acetate secretion rates. Contrary to what was expected from studies with a single strain in different conditions [17, 23, 24, 25], the model predicted no correlation between growth rate and acetate secretion rate in the case of different strains growing in the same environment, a result confirmed by the experimental data. A mapping from resource allocation to rate-yield phenotypes consistent with available proteomics data, however, could only be found when taking into account enzyme activities in addition to enzyme concentrations.

These results are interesting for both fundamental reseach and biotechnological applications. They show that the application of coarse-grained models can be used to predict multivariate phenotypes, without making any assumptions on optimality criteria, and reveal unexpected relations confirmed by the experimental data. The model is capable of predicting quantitative bounds on growth rates and yields within a specific environment, which can be exploited for rapidly screening performance limits of strains developed in synthetic biology and metabolic engineering.

Results

Coarse-grained model with coupled carbon and energy fluxes

Coarse-grained resource allocation models describe microbial growth by means of a limited number of macroreactions converting nutrients from the environment into proteins and other macromolecules. Several such models have been proposed, usually focusing on carbon fluxes [2, 4, 5, 6, 8, 9, 16]. The coupling of carbon and energy fluxes is essential for understanding the relation between growth rate and growth yield. Few models, however, have taken into account the energy balance of microbial growth, that is, the use of substrate for the production of ATP and other energy cofactors fueling macromolecular synthesis and cellular maintenance. Among the notable exceptions, we cite the model of Basan *et al.* [17, 19], which couples carbon and energy fluxes while abstracting from the reaction kinetics, and the model of Zavřel *et al.* [23], which does provide such a kinetic view while restricting biomass to proteins.

Figure 1 presents a coarse-grained kinetic model that takes inspiration from and generalizes upon this previous work. While the model is generic, it has been instantiated for aerobic growth of *E. coli* in minimal medium with glucose or glycerol as the limiting carbon source. The model variables comprise cellular concentrations of proteins (p) and other macromolecules (DNA, RNA, lipids, and polysaccharides) (u) as well as central carbon metabolites (c) and ATP (a^*). All concentrations have units Cmmol gDW^{-1}, except for ATP [mmol gDW^{-1}]. Five macroreactions are responsible for carbohydrate uptake and metabolism, ATP production by aerobic respiration and fermentation, and the synthesis of proteins and other macromolecules. The rates of the reactions, denoted by v_{mc}, v_{mer}, v_{mef}, v_r, and v_q [Cmmol gDW^{-1} h^{-1}], respectively, are defined by kinetic expressions involving protein, precursor metabolite, and energy cofactor concentrations. Details of the rate equations and the derivation of the model from basic assumptions on microbial growth can be found in Text S1.

The carbon entering the cell is included in the different biomass components or released in the form of CO_2 and acetate. CO_2 is produced by respiration and macromolecular synthesis, while acetate overflow is due to aerobic fermentation [17, 26]. The carbon balance also includes

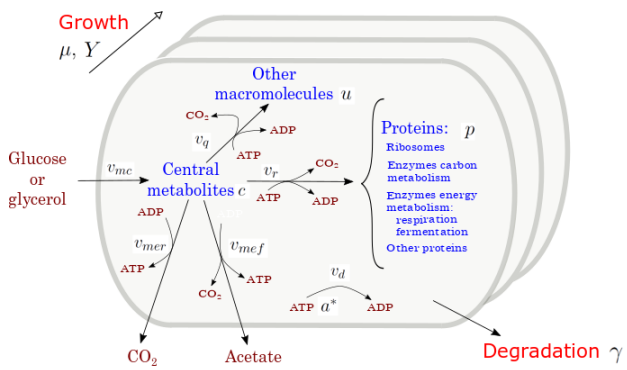

Carbon balance

$$\frac{dc}{dt} = v_{mc} - v_{mer} - \rho_{mef}\, v_{mef} - \rho_{rq}\,(v_r + v_q) - (\mu + \gamma)\, c$$
$$\frac{dp}{dt} = v_r - (\mu + \gamma)\, p$$
$$\frac{du}{dt} = v_q - (\mu + \gamma)\, u$$

Energy balance

$$\frac{da^*}{dt} = n_{mer}\, v_{mer} + n_{mef}\, v_{mef} - n_r\, v_r - n_q\, v_q - v_d$$

Growth rate and growth yield

$$\mu = \beta\,(v_{mc} - v_{mer} - \rho_{mef}\, v_{mef} - (\rho_{rq} - 1)\,(v_r + v_q)) - \gamma$$
$$Y = \frac{1}{\beta}\,\frac{\mu}{v_{mc}}$$

Resource allocation

$$\frac{dq}{dt} = \phi_q\, v_r - (\mu + \gamma)\, q$$
$$\frac{dr}{dt} = \phi_r\, v_r - (\mu + \gamma)\, r$$
$$\frac{dm_c}{dt} = \phi_c\, v_r - (\mu + \gamma)\, m_c$$
$$\frac{dm_{er}}{dt} = \phi_{er}\, v_r - (\mu + \gamma)\, m_{er}$$
$$\frac{dm_{ef}}{dt} = \phi_{ef}\, v_r - (\mu + \gamma)\, m_{ef}$$
$$1 = \phi_q + \phi_r + \phi_c + \phi_{er} + \phi_{ef}$$

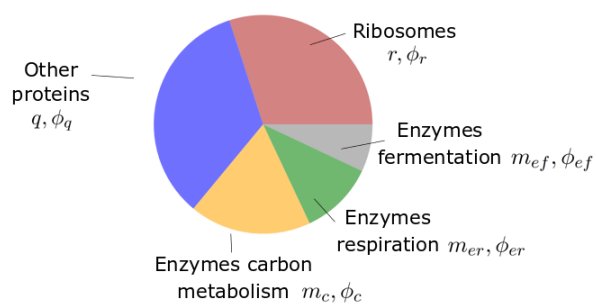

Figure 1: Coarse-grained model of microbial growth with coupled carbon and energy fluxes. Upper left figure: schematic outline of the model, showing the biomass constituents and the macroreactions, as wel as the growth and degradation of biomass. Green boxes: system of differential equations describing the carbon and energy balances, growth rate and growth yield, and resource allocation. The kinetic expressions for the reaction rates can be found in Text S1. The growth rate and growth yield are defined in terms of the fluxes of the macroreactions. Lower right figure: different protein categories considered in resource allocation. The fluxes v_r, v_q, v_{mc}, v_{mer}, v_{mef}, v_d [Cmmol or mmol gDW^{-1} h^{-1}], the variables p, r, q, m_c, m_{er}, m_{ef}, c, u, a^* [Cmmol or mmol gDW^{-1}], the resource allocation parameters ϕ_q, ϕ_r, ϕ_c, ϕ_{er}, ϕ_{ef} [dimensionless], the degradation rate constant γ [h^{-1}], the biomass density β [Cmmol gDW^{-1}], the ATP yield and cost factors n_{mer}, n_{mef}, n_r, n_q [mmol Cmmol^{-1}], and the CO_2 loss factors ρ_{mef}, ρ_{rq} [dimensionless] are formally defined in Text S1. The values of the parameters are derived in Text S2.

the turnover of macromolecules, which is responsible for a large part of cellular maintenance costs ([27] and Text S2).

The energy balance is expressed in terms of the production and consumption of ATP. While energy metabolism also involves other energy cofactors (NADP, NADPH, ...), the latter can be converted into ATP during aerobic growth [17, 26]. The ATP yields of respiration and fermentation (n_{mer} and n_{mef}) as well as the ATP costs of the synthesis of proteins and other macromolecules (n_r and n_q) are determined by the stoichiometry of the underlying metabolic pathways and the biomass composition ([17, 28] and Text S2). When total ATP production and consumption in growing microbial cells are computed from $n_{mer}\, v_{mer} + n_{mef}\, v_{mef}$ and $n_r\, v_r + n_q\, v_q$, respectively, the former usually largely exceeds the latter [29, 30]. This so-called uncoupling phenomenon is explicitly accounted for by an energy dissipation term v_d in the energy balance (Text S1).

Like in other resource allocation models, the proteome is subdivided into categories [2, 17]. We distinguish ribosomes and other translation-affiliated proteins, enzymes in central carbon metabolism, enzymes in respiration and fermentation metabolism, and other (housekeeping) proteins, with concentrations r, m_c, m_{er}, m_{ef}, and q, respectively. Each category of protein catalyzes a different macroreaction in Figure 1: ribosomes are responsible for protein synthesis, enzymes for carbon and energy metabolism, and housekeeping proteins for the synthesis of macromolecules other than proteins. The protein synthesis capacity of the cell, given by the total protein synthesis rate v_r, is distributed over the protein categories using five fractional resource allocation parameters that sum to 1: ϕ_q, ϕ_r, ϕ_c, ϕ_{er}, and ϕ_{ef}. Fixing the resource allocation parameters determines the model dynamics and therefore the growth phenotype [11, 23, 31].

Contrary to most models of microbial growth, the biomass includes other cellular components (DNA, RNA, metabolites, ...) in addition to proteins. The growth rate μ [h^{-1}] directly follows from the biomass definition, under the assumption that the total biomass concentration $1/\beta$ is constant ([32] and Text S1). The growth rate captures the specific accumulation of biomass corrected for maintenance:

$$\mu = \beta\,(v_{mc} - v_{mer} - \rho_{mef}\, v_{mef} - (\rho_{rq} - 1)\,(v_r + v_q)) - \gamma, \tag{1}$$

where ρ_{mef} and $\rho_{rq} - 1$ denote the fractional loss of CO_2 by fermentation and macromolecular synthesis, respectively. The growth yield is defined as the fraction of carbon taken up by the cells and included in the biomass:

$$Y = \frac{1}{\beta}\,\frac{\mu}{v_{mc}}. \tag{2}$$

Yields are dimensionless and vary between 0 and 1.

The model in Figure 1 was calibrated using data from the literature for batch or continuous growth of *E. coli* in minimal medium with glucose or glycerol. In brief, for the *E. coli* reference strain BW25113, we collected for each growth medium the growth rate and metabolite uptake and secretion rates [25, 33, 34], as well as protein and metabolite concentrations [18, 34, 35]. Using additional assumptions based on literature data, we fixed a unique set of parameters for each condition (batch *vs.* continuous growth, glucose *vs.* glycerol), without parameter fitting (Text S2). The resulting set of quantitative models provides a concise but comprehensive representation of microbial growth in different environments.

Predicted and observed rate-yield phenotypes for *Escherichia coli*

Using the model in Figure 1, we explored the effect of alternative resource allocation strategies on growth rate and growth yield. A resource allocation strategy is defined by the values for the resource allocation parameters: $(\phi_q, \phi_r, \phi_c, \phi_{er}, \phi_{ef})$ (Figure 2A). The medium-specific instantiations of the model were used to determine how the rate and yield change, within a given condition, when resource allocation is allowed to vary over the entire range of possible strategies. We therefore uniformly sampled the space of possible combinations of resource allocation parameters, while keeping the fraction attributed to housekeeping proteins ϕ_q constant [2]. The model was considered at steady state, corresponding to balanced growth of the culture. The steady state for each resource allocation strategy was determined numerically (*Methods*).

Figure 2B-C shows the space of possible rate-yield phenotypes for batch growth on glucose or glycerol. A first observation is that the predicted combinations of rate and yield are bounded. The growth rate does not exceed 1.1 h^{-1}, and for all but the lowest growth rates, the growth yield is larger than 0.3. A second observation is that, for low growth rates, the maximum growth yield increases with the rate, whereas it decreases for high growth rates. The initial yield increase is due to the proportionally lower burden of the maintenance costs at higher growth rates [36]. The subsequent decrease of the maximum yield reflects a trade-off that has been much investigated in microbial physiology and ecology [37, 38].

The model predictions can be directly compared with experimental data. We compiled a database of measured rates and yields reported in the literature for growth of *E. coli* in minimal medium with glucose or glycerol (Files S1 and S2), and plotted the measurements in the predicted phenotype spaces (Figure 2B-C). The database includes the reference wild-type strain used for model calibration (BW25113), other *E. coli* wild-type strains, strains with mutants in regulatory genes, and strains obtained from ALE experiments. Apart from the rate and yield of the reference strain [33], none of the data points plotted in Figure 2B-C were used for calibration.

The measured rates and yields correspond very well with the model predictions: almost all data points fall inside the predicted phenotype space and much of the space is covered by the data points. The range of high growth rates is enriched in data points, which reflects the bias that *E. coli* wild-type and mutant strains grow relatively fast on glucose and glycerol, and that in most ALE experiments the selection pressure is tilted towards growth rate. Interestingly, the highest growth rates on glucose attained in ALE experiments, just above 1 h^{-1} [21, 39], agree quite well with the highest predicted growth rates.

The BW25113 strain used for calibration has a low growth yield on glucose (equal to 0.50, [33]). Many deletion mutants of regulatory genes somewhat increase that yield [33], but still fall well below the maximally predicted yield. The growth yield of some other wild-type strains is significantly higher, for example the W strain achieves a yield of 0.66 at a growth rate of 0.97 h^{-1} [20]. The highest growth yield is achieved by an evolved strain (0.81, [40]), agreeing quite well with the maximum predicted growth yield for that growth rate. The latter strain does not secrete any acetate while growing on glucose [40], which contributes to the higher yield.

Similar observations can be made for growth of *E. coli* on glycerol, although in this case less experimental data points are available. The model predicts that the highest growth rate on glycerol is close to the highest growth rate on glucose, which is confirmed by experimental

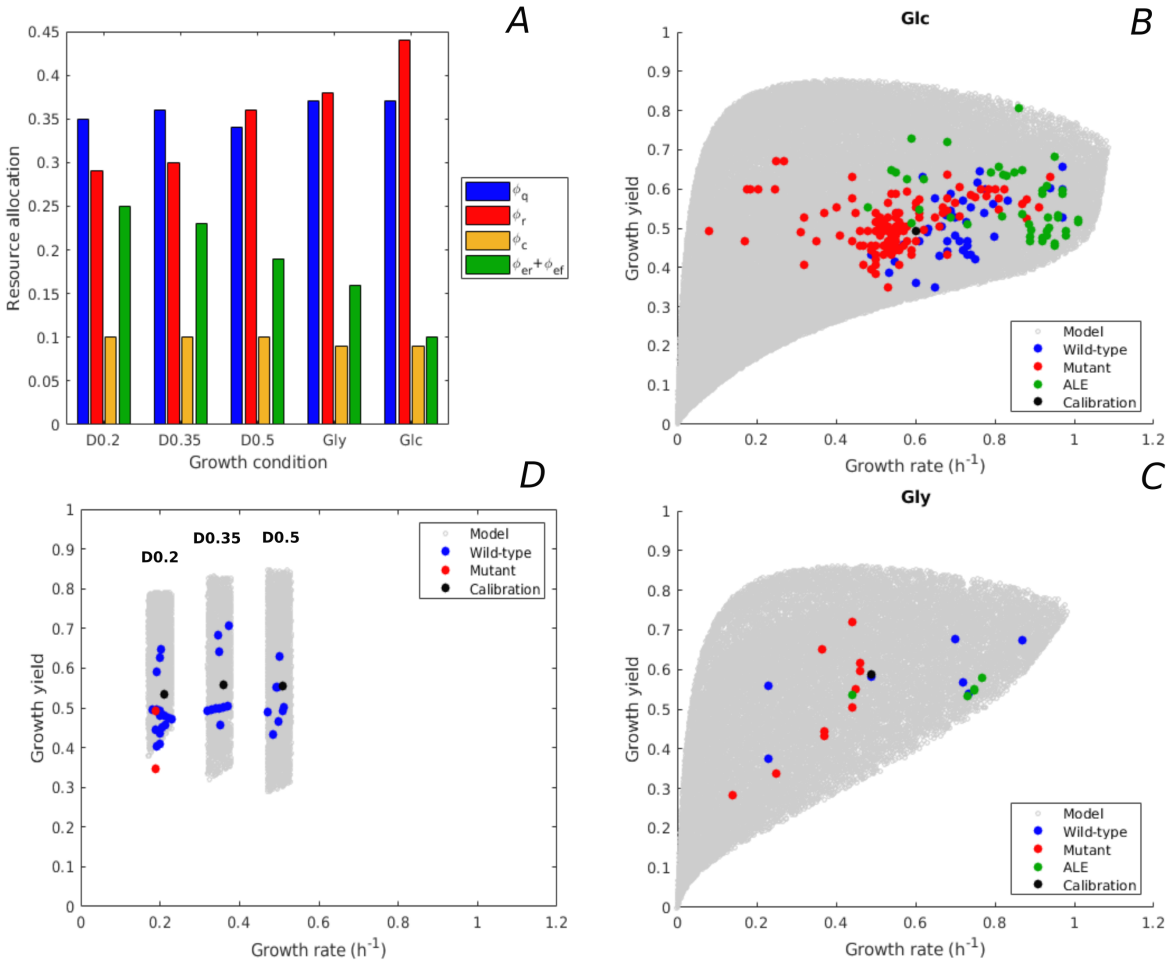

Figure 2: Predicted rate-yield phenotype space and comparison with experimental data. **A.** Measured proteome fractions of the protein categories in the model (resource allocation strategies) for the BW25113 reference strain used for calibration ([18], see Text S2). **B.** Predicted and observed combinations of growth rate and growth yield for steady-state batch growth of *E. coli* in minimal medium with glucose. The rate-yield phenotypes concern the reference strain, other wild-type strains, mutant strains obtained by directed mutagenesis, and mutant strains from ALE experiments. **C.** Idem for batch growth of *E. coli* in minimal medium with glycerol. **D.** Idem for continuous growth in a chemostat of *E. coli* in minimal medium with glucose at different dilution rates (0.2, 0.35, and 0.5 h^{-1}). The predicted yields are shown for the dilution rates ±10%. All predictions were made using the model in Figure 1, calibrated for the different growth conditions, and varying the resource allocation parameters between 0 and 1, except ϕ_q (40,000-90,000 samples). The measurements of rate and yield reported in the source literature have been converted to units h^{-1} (growth rate) and a dimensionless unit corresponding to $\text{Cmmol}_{\text{biomass}}$ $\text{Cmmol}^{-1}_{\text{substrate}}$ (growth yield) (see Text S1 and Files S1 and S2 for details).

data [41]. In addition to batch growth, we also considered continuous growth in a chemostat. This required a recalibration of the model, since the environment is not the same as for batch growth (Text S2). Figure 2D shows the predicted rate-yield phenotype space for dilution rates around 0.2, 0.35, and 0.5 h^{-1}, as well as the observed rates and yields. Again, there is good correspondence between model and data. Most chemostat experiments reported in the literature have been carried out with the BW25113 and MG1655 wild-type strains. This absence of mutants and evolved strains may lead to an underestimation of the range of observed growth yields.

In the above comparisons of the model with the data, we made the assumption that the strains considered have the same metabolic capacities as the reference strain. That is, they utilize the same pathways in central carbon and energy metabolism to convert substrate into precursor metabolites and ATP. This assumption was satisfied by restricting the database to wild-type strains with essentially the same central carbon and energy metabolism [20], mutant strains with deletions of genes encoding regulators instead of enzymes [33], and short-term ALE mutants which have not had the time to develop new metabolic capacities [39]. We also made the assumption that the parameter values are the same for all strains, so that differences in resource allocation strategies are the only explanatory variable. It is remarkably that, despite this strong assumption, the model of Figure 1 accounts very well for the observed variability of rate-yield phenotypes in *E. coli*.

Predicted and observed flux phenotypes for *Escherichia coli*

Growth rate and growth yield are defined in terms of carbon and energy fluxes through the population (Eqs. 1 and 2). Like rate and yield, some of these fluxes, in particular uptake and secretion rates, have been found to largely vary across *E. coli* strains growing in minimal medium with glucose [20, 21]. Can our model also reproduce the observed flux variability? We compared the model predictions of the uptake and secretion rates with their measurements, when available (File S1).

Figure 3A-B shows the projection of the predicted and measured glucose uptake rates on the rate-yield phenotype space. The correspondence of the model and the data is very high: more than 90% of the variance is captured by the model (Figure S1). This high correlation is not surprising. For a given growth rate μ and growth yield Y, the glucose uptake rate v_{mc} is determined by the relation in Eq. 2. What the correspondence shows is that the total biomass concentration $1/\beta$ does not vary much across the different strains, agreeing with what was observed for steady-state growth of a given *E. coli* strain in different media [42, 43].

Another observable flux phenotype is the acetate secretion rate, which is an indicator of the functioning of energy metabolism. In aerobic conditions, *E. coli* has two different modes of ATP production: respiration and fermentation. Glucose and glycerol are taken up by the cells and degraded in the glycolysis pathway, eventually producing acetyl-CoA. Whereas acetyl-CoA enters the tricarboxylic acid (TCA) cycle in the case of respiration, it is secreted in the form of acetate during fermentation. In both cases, NADP and other reduced compounds are produced along the way and their recycling is coupled with the generation of a proton gradient across the membrane, enabling the production of ATP. Respiration is the more efficient of the two ATP production modes: in *E. coli*, respiration yields 26 ATP molecules per molecule of glucose and fermentation only 12 [17].

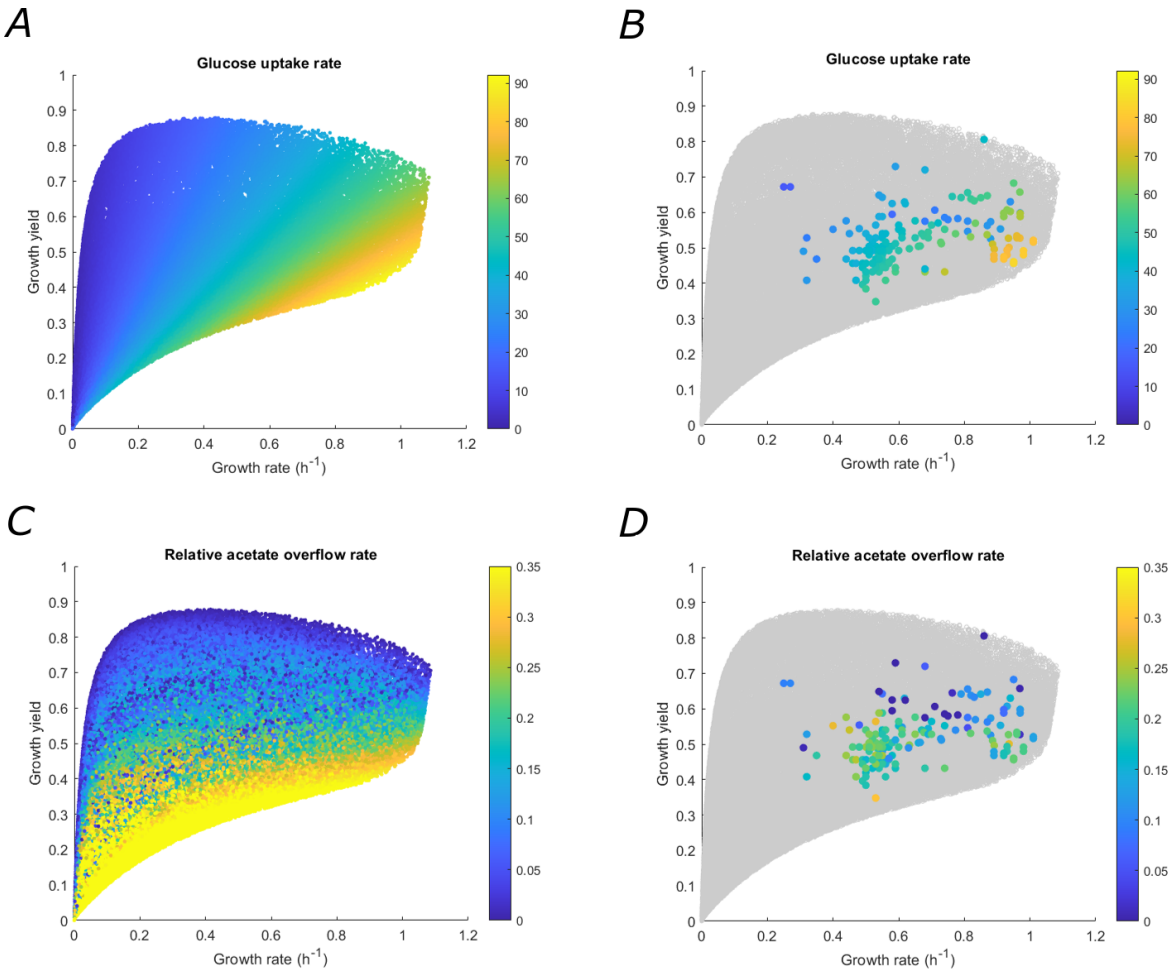

Figure 3: Predicted flux phenotypes and comparison with experimental data. A. Glucose uptake rate (v_{mc}) for every predicted rate-yield combination in the case of batch growth of *E. coli* on minimal medium with glucose (Figure 2B). **B.** Idem for measured combinations of glucose uptake rate, growth rate, and growth yield (File S1). The predicted and observed secretion rates are strongly correlated ($R^2 = 0.93$, Figure S1), in agreement with Eq. 2. **C.** Relative acetate secretion rate (v_{mef}/v_{mc}) for every predicted rate-yield combination. **D.** Idem for measured combinations of glucose uptake rate, acetate secretion rate, growth rate, and growth yield (File S1). The predicted and observed relative acetate secretion rates are correlated ($R^2 = 0.66$, Figure S1). There is no evidence in the data of a correlation between growth rate and relative acetate secretion rate ($R^2 = 0.08$, Figure S1). In addition to the relative acetate overflow, the model also captures the absolute acetate overflow very well (Figure S2).

How does the contribution of fermentation to ATP production change over the rate-yield phenotypes? Contrary to the glucose uptake rate, the growth rate and growth yield do not uniquely determine the acetate overflow rate v_{mef} (Eqs. 1 and 2). Instead, the acetate overflow rate is the consequence of the resource allocation strategy adopted by the cell. We examined the predicted and observed contributions of fermentation to ATP production in the case of batch growth on glucose. In particular, we quantified the extent of fermentation by the relative rate of acetate overflow, that is, the fraction of carbon taken up that is secreted as acetate (v_{mef}/v_{mc}). As shown in Figure 3C, over almost the entire range of growth rates, a continuum of ATP production, from pure respiration to combinations of respiration and fermentation, is possible according to the model. However, the ATP production mode is directly correlated with the growth yield. Maximum yield requires respiration without fermentation, whereas minimum yield is attained for maximum fermentation, where more than 30% of the carbon entering the cell is lost due to acetate overflow.

The predicted pattern of the variation of acetate overflow over the rate-yield phenotype space is largely confirmed by the experimental data (Figure 3D). Some of the fastest growing *E. coli* wild-type strains have no acetate overflow, like the W strain [20], while some of the evolved strains grow very fast but with little acetate overflow as compared to their ancestors [40]. Respiration phenotypes are over-represented at high growth yields, over the whole range of growth rates, whereas fermentation phenotypes are associated with low growth yields. The model accounts for maximally 66% of the variance of the observed relative acetate overflow (Figure S1). This correspondence may be underestimated due to a bias in our definition of fermentation phenotypes, which is based on acetate overflow only and does not take into account the possible secretion of other by-products (formate, succinate, lactate, ...). Overflow of other fermentation products is known to occur during batch growth on glucose, especially for mutants [44, 45, 46].

Given the higher ATP yield of respiration, it is not surprising that the highest growth yields are obtained when respiration is preferred to fermentation. What might not have been expected, however, is that resource allocation strategies enabling cells to bypass fermentation at high growth rates are possible at all. It is well-known that, when growing an *E. coli* strain in different environments supporting increasingly higher growth rates, the contribution of fermentation to ATP production increases at the expense of respiration, as witnessed by the relative increase of acetate secretion ([17] and Figure S3). In the scenario considered here, however, both the model and the data suggest that there exist strategies enabling strains to attain growth rates close to the maximum without shifting resources from respiration to fermentation.

Differences in enzyme activity are necessary to explain variations in protein abundance

The simple model of Figure 1 accounts remarkably well for the variability of observed rate-yield and flux phenotypes in *E. coli*. It raises the question how the phenotypes are related to the underlying resource allocation strategies. This relation is not straightforward due to the multiple feedback loops in the model, which entail strong mutual dependencies between carbon and energy metabolism, protein synthesis, and growth. Figure S4 shows the mapping from resource allocation strategies to rate-yield phenotypes in the case of batch growth on glucose.

Whereas every strategy gives rise to a unique rate-yield phenotype (*Methods*), the inverse is not true: infinitely many strategies can account for a given growth rate and growth yield. Intuitively, by Eqs. 1 and 2, a given rate-yield phenotype fixes the substrate uptake rate v_{mc} and the sum $v_{mer} + \rho_{mef}\, v_{mef} + (\rho_{rq} - 1)\,(v_r + v_q))$, representing the loss of carbon due to CO_2 outflow and acetate secretion. Different protein concentrations can lead to fluxes that add up to the latter sum, and thus enable the cells to grow at the specified rate and yield (Figure S4).

How do the resource allocation strategies underlying a given rate-yield phenotype compare with those actually observed? Unfortunately, for most of the strains in the database, other than the BW25113 strain used for calibration, no proteomics data are available. Exceptions are the other commonly-used wild-type strains MG1655 and NCM3722 [18]. Schmidt *et al.* found growth rates equal to 0.67 h^{-1} and 1.03 h^{-1} for MG1655 and NCM3722, respectively [18]. Growth yields reported by other groups for these strains, in the same conditions with approximately the same growth rates, are 0.54 for MG1655 and 0.6 for NCM3722 [47, 48]. We compared resource allocation strategies predicting the above rates and yields with those actually observed for MG1655 and NCM3722 (*Methods*).

As seen in Figure 4A, there exist strategies predicting growth at approximately the same rate and yield as MG1655 that fall within a 10% margin of the experimental values. This indicates that the model accounts for the observed strategy of a strain with a similar growth phenotype as the BW25113 strain. NCM3722 grows much faster and at a higher yield than BW25113. Whereas there exist strategies with a good correspondence for the ribosomal protein fraction ϕ_r, the predicted ϕ_c values for a strain with the same rate and yield as NCM3722 are much higher than those observed (Figure 4B). In other words, the model predicts a higher protein fraction for enzymes in central carbon metabolism (m_c/p) than observed in the proteomics data. The underlying problem is that in our model the carbon uptake and metabolization rate is directly proportional to the enzyme concentration ($v_{mc} = k_{mc}\, m_c\, S/(S + K_{mc})$, where k_{mc} [h^{-1}] is an environment-dependent apparent catalytic constant and S the constant substrate concentration, Text S1). Therefore, an increase in v_{mc} necessary for the higher growth rate of the NCM3722 strain, requires a proportional increase in enzyme concentration, and causes the protein fraction m_c/p to increase. The measured protein fraction, however, remains approximately stable (0.09 for BW25113 and 0.07 for NCM3722). A similar but opposite divergence of model and data is seen in the case of the protein fraction of enzymes in energy metabolism (Figure 4B).

Resource allocation explains the protein fraction of ribosomes necessary to attain the observed rate and yield. The discrepancies between predicted and observed enzyme fractions, however, show that additional regulatory factors need to be considered in the latter case. This conclusion agrees with the widespread view that the regulation of fluxes in central metabolism is largely due to the regulation of enzyme activity rather than enzyme concentrations [49, 50]. While little is known about the mechanisms allowing NCM3722 to grow much faster than BW25113, genomic changes and their physiological impact have been identified for ALE strains [21, 22, 51]. In an ALE mutant evolved in glycerol, the change in growth rate was attributed to a change in activity of the GlpK enzyme [51], leading to higher glycerol uptake rates. In the model, the latter mutation would translate to an increase in the catalytic constant k_{mc} (Text S1).

In order to verify the hypothesis that changes in kinetic parameters can restore the consistency between predicted and observed enzyme concentrations, we modified the analysis of

the model. Instead of varying only resource allocation parameters ($\phi_q, \phi_r, \phi_c, \phi_{er}, \phi_{ef}$), we also allowed the catalytic constants (k_{mc}, k_{mer}, k_{mef}), representing the (apparent) enzyme turnover rates in central carbon and energy metabolism (Text S1), to increase or decrease by at most a factor of 2. The results of the simulations are shown in Figure 4C-D. For both the MG1655 and NCM3722 strains, there now exist resource allocation strategies and corresponding protein fractions consistent with the experimental data within a 5% margin. The NCM3722 strategies display an increased value of k_{mc} (Figure S5). That is, the model predicts that glycolytic enzymes are more active in NCM3722 as compared to BW25113 during growth on glucose. As a consequence, resources can be shifted from glycolytic enzymes to other proteins and metabolites, which allows the growth rate and yield to increase. While resource allocation provides quantitative bounds on growth rate, growth yield, and uptake and secretion rates agreeing with the experimental data, quantitatively correct predictions of protein concentrations therefore require metabolic regulation to be taken into account as well.

Discussion

Analysis of the resource allocation strategies adopted by microbial cells can explain a number of phenomenological relations between growth rate, growth yield, and macromolecular composition [2, 3, 4, 5, 6, 7, 8, 9, 10, 11]. We have generalized this perspective to account for a striking observation: the large variability of rate-yield phenotypes across different strains of a bacterial species grown in the same environment. We constructed a coarse-grained resource allocation model (Figure 1), which was calibrated using literature data on batch and continuous growth of *E. coli* in minimal medium with glucose or glycerol. In each of the conditions, we considered the space of rate-yield phenotypes predicted by the model when allowing resource allocation to vary over the entire range of possible strategies, while keeping the kinetic parameters constant.

This approach is based on a number of strong assumptions. The coarse-grained nature of the model reduces microbial metabolism and protein synthesis to a few macroreactions, instead of accounting for the thousands of enzyme-catalyzed reactions involved in these processes [48, 52, 53]. Resource allocation is reduced to constraints on protein synthesis capacity, whereas other constraints such as limited solvent capacity and membrane space may also play a role [52, 54, 55, 56]. All possible combinations of resource allocation parameters were considered, limited only by the constraint that they must sum to 1. Observed variations in protein abundance are less drastic [18, 57], and coupled through shared regulatory mechanisms [3, 58]. The kinetic parameters in the model have apparent values absorbing unknown regulatory effects, specific to each growth condition. This contrasts with strain-specific kinetic models with an explicit representation of the underlying regulatory mechanisms [6, 59, 60], and does not allow our model to be used for transitions between growth conditions.

Despite these limitations, we observed a very good quantitative correspondence between the predicted and the measured rate-yield phenotypes across different *E. coli* strains grown in the same environment (Figure 2). This suggests that differences in resource allocation are a major explanatory factor for the observed rate-yield variability. We also found a surprising absence of correlation between growth rate and relative acetate overflow (Figure 3 and Figure S1), contrary to what has been observed for a single strain in different conditions (Figure S3). This observation,

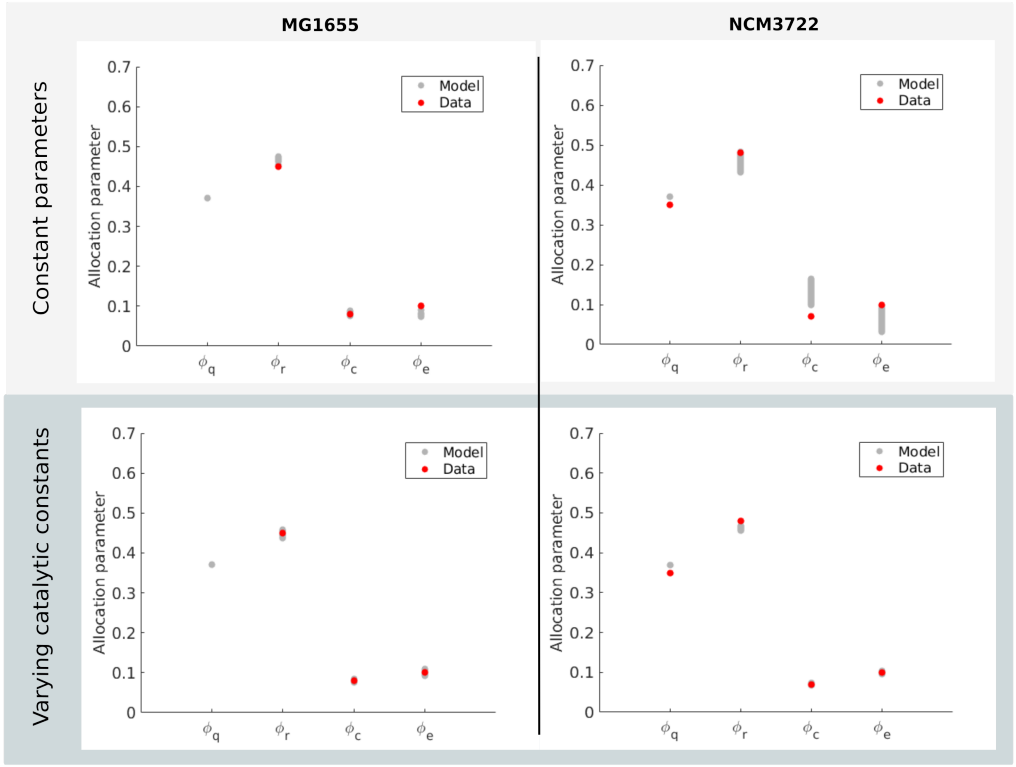

Figure 4: Validation of predicted resource allocation strategies by means of proteomics data. **A.** Observed research allocation strategy for batch growth of the MG6155 strain in minimal medium with glucose [18] (red dots) as well as examples of resource allocation strategies giving a similar growth rate and growth yield in the simulations of Figure 2B (grey dots). The predicted growth yield Y, growth rate μ, and resource allocation parameters $\phi_q, \phi_r, \phi_c, \phi_{er} + \phi_{ef}$ are each allowed to vary by less than 10% from the observed values. **B.** Idem for the NCM3722 strain, without imposing ϕ_c and $\phi_{er} + \phi_{ef}$ to agree with the experimental data. The actually observed strategies do not match the predicted strategies in the case of NCM3722. **C.** As in panel A, but allowing the apparent catalytic constants (k_{mc}, k_{mer}, k_{mef}) to vary by a factor of 2 in comparison with the reference values determined for the BW25113 strain (Text S2). The discrepancy between the predicted and observed strategies is set to a 5% limit. **D.** Idem for the NCM3722 strain. When relaxing the constraint of constant kinetic parameters, the model agrees with the observed resource allocation strategies of both MG6155 and NCM3722. This requires an increase of k_{mc} and a decrease of k_{mef} (Figure S5).

which was made before for a selection of ALE mutant strains [48], raises several questions. First, why is a shift of resources from respiration to fermentation, reflecting a trade-off between energy efficiency and protein cost [4, 17, 61], not required for obtaining a higher growth rate? We inspected the strategies producing a high growth rate and little acetate overflow, and compared these with resource allocation in the reference strain used for calibration. For example, high rate-high yield strains limit their investment in ribosomes, but increase concentrations of metabolic precursors and/or energy cofactors to maintain high protein synthesis fluxes (Figure S6). This suggests a trade-off reminiscent of the hypothesized trade-off between enzyme and metabolite concentrations in central carbon metabolism [62, 63]. Second, why do most *E. coli* strains in Figure 3 nevertheless display acetate overflow and grow at a suboptimal yield? The answer is not known, but probably relates to the natural environment in which *E. coli* has evolved, characterized by periodic anoxic conditions and synthrophic interactions with other species [64].

When comparing the predicted resource allocation strategies with those observed for a given rate and yield (Figure 5A-B), we found some discrepancies that cannot be solely attributed to the uncertainty in the proteomics data. In particular, the concentrations of enzymes in central carbon metabolism are consistently overestimated by the model for rates and yields exceeding those observed for the BW25113 reference strain, due to the assumption that the kinetic parameters are constant. When allowing the catalytic constants of the metabolic macroreaction to vary as well, we could restore consistency between the model and the data (Figure 5). Further investigation indicated that in strains attaining a higher growth rate and yield than the BW25113 strain, glycolytic enzymes must be more active. To our knowledge, no experimental data exist to specifically test this prediction. It is known, however, that the activity of pyruvate kinase, regulated by fructose-1,6-bisphosphate [65], increases with a higher glycolytic flux [66, 67]. In other words, a higher growth rate is accomplished at a higher activity of this glycolytic enzyme.

We conclude that the assumption that resource allocation alone can explain the observed rate-yield variability is a good first approximation that can be refined by taking into account differences in enzyme activity, either due to genetic differences between strains or to regulatory mechanisms responding to physiological changes. Predictions of the range of rates and yields achievable by a microbial species, and relating these to underlying resource allocation strategies, are of great interest for a fundamental understanding of microbial growth. In addition, by extending the model with a macroreaction for the production of a protein or a metabolite of interest [68], this provides rapidly exploitable guidelines for metabolic engineering and synthetic biology, by pointing at performance limits of specific strains and suggesting improvements. While instantiated for growth of *E. coli*, the model equations are sufficiently generic to apply to other microorganisms. The calibration of such model variants can benefit from the same hierarchical procedure as developed here, exploiting largely available proteomics and metabolomics datasets.

Methods

The resource allocation models were derived from a limited number of assumptions on the processes underlying microbial growth, as explained in Text S1. The parameters in the models were determined from literature data, as described in Text S2. In order to produce the rate-yield phenotype plots, we uniformly sampled combinations of resource allocation parameters ϕ_r, ϕ_c,

ϕ_{er}, and ϕ_{ef} such that their sum equals 1-ϕ_q, where ϕ_q was set to a constant value determined from the data (Text S2). Starting from initial conditions, the system was simulated for each combination of resource allocation parameters until a steady state was reached. When sampling the space of initial conditions for several resource allocation strategies, the system was found to always reach the same steady state. All simulations were carried out by means of Matlab R2020b. The models and the simulation code used for generating all figures in the paper are available as File S4.

The rate-yield database was compiled from the experimental literature (Files S1 and S2). When yields were explicily reported, they were converted to the dimensionless quantity $\text{Cmmol}_{\text{substrate}}$ $\text{Cmmol}^{-1}_{\text{biomass}}$ used in this paper, using appropriate conversion constants (Text S1). The relative acetate secretion flux was computed for those studies in the database in which both the glucose uptake rate and the acetate secretion rate were measured. Both rates were converted into the appropriate unit (Cmmol gDW^{-1} h^{-1}).

The comparison of predicted and observed resource allocation strategies for the BW25113, MG1655 and NCM3722 strains was carried out by means of the proteomics data of Schmidt *et al.* ([18], Table S11). We computed the mass fraction for each protein category distinguished in the model by associating the latter with specific COG groups ($r/p \rightarrow$ Amino acid transport and metabolism and Translation; $m_c/p \rightarrow$ Carbohydrate transport and metabolism; $(m_{er} + m_{ef})/p \rightarrow$ Energy production and conversion; $q/p \rightarrow$ All other COG groups). The mass fraction of enzymes in energy metabolism was further subdivided into fractions attributed to respiration and fermentation, m_{er}/p and m_{ef}/p, in the same way as for model calibration, by distinguishing enzymes specific to fermentation, enzymes specific to respiration, and enzymes shared between respiration and fermentation ([17] and File S3). The resource allocation strategy $(\phi_q, \phi_r, \phi_c, \phi_{er}, \phi_{ef})$ was equated with the corresponding mass fractions.

Supporting information

Text S1. Model equations (pdf file).

Text S2. Model calibration (pdf file).

Figure S1-S6. Supplementary figures (pdf file).

File S1. Database with reported rate-yield pairs for *E. coli* grown on glucose minimal medium (excel file).

File S2. Database with reported rate-yield pairs for *E. coli* grown on glycerol minimal medium (excel file).

File S3. Classification of energy proteins (excel file).

File S4. Matlab code (zip file).

Acknowledgments

This work was supported by the ANR project Maximic (ANR-17-CE40-0024). The authors would like to thank Francis Mairet and Antrea Pavlou for comments on a previous version of the manuscript.

References

[1] M. Schachter, J. Ingraham, and F. Neidhardt, Microbe. Washington, DC: ASM Press, 2006.

[2] M. Scott, C. Gunderson, E. Mateescu, Z. Zhang, and T. Hwa, "Interdependence of cell growth and gene expression: Origins and consequences," Science, vol. 330, no. 6007, pp. 1099–1103, 2010.

[3] M. Scott, S. Klumpp, E. Mateescu, and T. Hwa, "Emergence of robust growth laws from optimal regulation of ribosome synthesis," Mol. Syst. Biol., vol. 10, p. 747, 2014.

[4] D. Molenaar, R. van Berlo, D. de Ridder, and B. Teusink, "Shifts in growth strategies reflect tradeoffs in cellular economics," Mol. Syst. Biol., vol. 5, p. 323, 2009.

[5] N. Giordano, F. Mairet, J.-L. Gouzé, J. Geiselmann, and H. de Jong, "Dynamical allocation of cellular resources as an optimal control problem: Novel insights into microbial growth strategies," PLoS Comput. Biol., vol. 12, no. 3, p. e1004802, 2016.

[6] A. Weiße, D. Oyarzún, V. Danos, and P. Swain, "Mechanistic links between cellular trade-offs, gene expression, and growth," Proc. Natl. Acad. Sci. USA, vol. 112, no. 9, pp. E1038–47, 2015.

[7] A. Reimers, H. Knoop, A. Bockmayr, and R. Steuer, "Cellular trade-offs and optimal resource allocation during cyanobacterial diurnal growth," Proc. Natl. Acad. Sci. USA, vol. 114, no. 31, pp. E6457–65, 2017.

[8] E. Bosdriesz, D. Molenaar, B. Teusink, and F. Bruggeman, "How fast-growing bacteria robustly tune their ribosome concentration to approximate growth-rate maximization," FEBS J., vol. 282, no. 10, pp. 2029–2044, 2015.

[9] B. Towbin, Y. Korem, A. Bren, S. Doron, R. Sorek, and U. Alon, "Optimality and sub-optimality in a bacterial growth law," Nat. Commun., vol. 8, p. 14123, 2017.

[10] A. Maitra and K. Dill, "Bacterial growth laws reflect the evolutionary importance of energy efficiency," Proc. Natl. Acad. Sci. USA, vol. 112, no. 2, pp. 406–11, 2015.

[11] H. Dourado and M. Lercher, "An analytical theory of balanced cellular growth," Nat. Commun., vol. 11, no. 1, p. 1226, 2020.

[12] E. Metzl-Raz, M. Kafri, G. Yaakov, I. Soifer, Y. Gurvich, and N. Barkai, "Principles of cellular resource allocation revealed by condition-dependent proteome profiling," eLife, vol. 6, p. e28034, 2017.

[13] J. Forchhammer and L. Lindahl, "Growth rate of polypeptide chains as a function of the cell growth rate in a mutant of *Escherichia coli* 15," J. Mol. Biol., vol. 55, no. 3, pp. 563–8, 1971.

[14] H. Bremer and P. Dennis, "Modulation of chemical composition and other parameters of the cell by growth rate," in *Escherichia coli* and *Salmonella*: Cellular and Molecular Biology (F. Neidhardt, R. Curtiss III, J. Ingraham, E. Lin, K. Low, B. Magasanik, W. Reznikoff, M. Riley, M. Schaechter, and H. Umbarger, eds.), pp. 1553–1569, Washington, DC: ASM Press, 2nd ed., 1996.

[15] S. Herendeen, R. VanBogelen, and F. Neidhardt, "Levels of major proteins of *Escherichia coli* during growth at different temperatures," J. Bacteriol., vol. 139, no. 1, pp. 185–94, 1979.

[16] F. Mairet, J.-L. Gouzé, and H. de Jong, "Optimal proteome allocation and the temperature dependence of microbial growth laws," npj Syst. Biol. Appl., vol. 7, p. 14, 2021.

[17] M. Basan, S. Hui, H. Okano, Z. Zhang, Y. Shen, J. Williamson, and T. Hwa, "Overflow metabolism in *Escherichia coli* results from efficient proteome allocation," Nature, vol. 528, no. 7580, pp. 99–104, 2015.

[18] A. Schmidt, K. Kochanowski, S. Vedelaar, E. Ahrné, B. Volkmer, L. Callipo, K. Knoops, M. Bauer, R. Aebersold, and M. Heinemann, "The quantitative and condition-dependent *Escherichia coli* proteome," Nat. Biotechnol., vol. 34, no. 1, pp. 104–10, 2016.

[19] M. Mori, E. Marinari, and A. D. Martino, "A yield-cost tradeoff governs *Escherichia coli*'s decision between fermentation and respiration in carbon-limited growth," NPJ Syst. Biol. Appl., vol. 5, p. 16, 2019.

[20] J. Monk, A. Koza, M. Campodonico, D. Machado, J. Seoane, B. Palsson, M. Herrgøard, and A. Feist, "Multi-omics quantification of species variation of *Escherichia coli* links molecular features with strain phenotypes," Cell Syst., vol. 3, no. 3, pp. 238–51, 2016.

[21] R. LaCroix, T. Sandberg, E. O'Brien, J. Utrilla, A. Ebrahim, G. Guzman, R. Szubin, B. Palsson, and A. Feist, "Use of adaptive laboratory evolution to discover key mutations enabling rapid growth of *Escherichia coli* K-12 MG1655 on glucose minimal medium," Appl. Environ. Microbiol., vol. 81, no. 1, pp. 17–30, 2015.

[22] J. Utrilla, E. O'Brien, K. Chen, D. McCloskey, J. Cheung, H. Wang, D. Armenta-Medina, A. Feist, and B. Palsson, "Global rebalancing of cellular resources by pleiotropic point mutations illustrates a multi-scale mechanism of adaptive evolution," Cell Syst., vol. 2, no. 4, pp. 260–71, 2016.

[23] T. Zavřel, M. Faizi, C. Loureiro, G. Poschmann, K. Stühler, M. Sinetova, A. Zorina, R. Steuer, and J. Červenó, "Quantitative insights into the cyanobacterial cell economy," Elife, vol. 8, p. e42508, 2019.

[24] A. Nanchen, A. Schicker, and U. Sauer, "Nonlinear dependency of intracellular fluxes on growth rate in miniaturized continuous cultures of *Escherichia coli*," Appl. Environ. Microbiol., vol. 72, no. 2, pp. 1164–72, 2006.

[25] K. Peebo, K. Valgepea, A. Maser, R. Nahku, K. Adamberg, and R. Vilu, "Proteome reallocation in *Escherichia coli* with increasing specific growth rate," Mol. Biosyst., vol. 11, no. 4, pp. 1184–1193, 2015.

[26] G. Gottschalk, Bacterial Metabolism. New York: Springer, 2nd ed., 1986.

[27] P. van Bodegom, "Microbial maintenance: a critical review on its quantification," Microb. Ecol., vol. 53, no. 4, pp. 513–23, 2007.

[28] C. Kaleta, S. Schäuble, U. Rinas, and S. Schuster, "Metabolic costs of amino acid and protein production in *Escherichia coli*," Biotechnol. J., vol. 8, no. 9, pp. 1105–14, 2013.

[29] A. Feist, C. Henry, L. Reed, M. Krummenacker, A. Joyce, P. Karp, L. Broadbelt, V. Hatzimanikatis, and B. Palsson, "A genome-scale metabolic reconstruction for *Escherichia coli* K-12 MG1655 that accounts for 1260 ORFs and thermodynamic information," Mol. Syst. Biol., vol. 3, p. 121, 2007.

[30] J. Russell and G. Cook, "Energetics of bacterial growth: balance of anabolic and catabolic reactions," Microbiol. Rev., vol. 59, no. 1, pp. 48–62, 1995.

[31] D. de Groot, J. Hulshof, B. Teusink, F. Bruggeman, and R. Planqué, "Elementary Growth Modes provide a molecular description of cellular self-fabrication," PLoS Comput. Biol., vol. 16, no. 1, p. e1007559, 2020.

[32] H. de Jong, S. Casagranda, N. Giordano, E. Cinquemani, D. Ropers, J. Geiselmann, and J.-L. Gouzé, "Mathematical modelling of microbes: metabolism, gene expression and growth," J. R. Soc. Interface, vol. 14, no. 136, p. 2017050, 2017.

[33] B. H. van Rijsewijk, A. Nanchen, S. Nallet, R. Kleijn, and U. Sauer, "Large-scale L13C-flux analysis reveals distinct transcriptional control of respiratory and fermentative metabolism in *Escherichia coli*," Mol. Syst. Biol., vol. 7, p. 477, 2011.

[34] L. Gerosa, B. H. van Rijsewijk, D. Christodoulou, K. Kochanowski, T. Schmidt, E. Noor, and U. Sauer, "Pseudo-transition analysis identifies the key regulators of dynamic metabolic adaptations from steady-state data," Cell Syst., vol. 1, no. 4, pp. 270–82, 2015.

[35] B. Bennett, E. Kimball, M. Gao, R. Osterhout, S. V. Dien, and J. Rabinowitz, "Absolute metabolite concentrations and implied enzyme active site occupancy in *Escherichia coli*," Nat. Chem. Biol., vol. 5, no. 8, pp. 593–599, 2009.

[36] S. Pirt, "The maintenance energy of bacteria in growing cultures," Proc. R. Soc. Lond. B Biol. Sci., vol. 163, no. 991, pp. 224–31, 1965.

[37] D. Lipson, "The complex relationship between microbial growth rate and yield and its implications for ecosystem processes," Front. Microbiol., vol. 6, p. 615, 2015.

[38] R. Beardmore, I. Gudelj, D. Lipson, and L. Hurst, "Metabolic trade-offs and the maintenance of the fittest and the flattest," Nature, vol. 472, no. 7343, pp. 342–6, 2011.

[39] J. Monk, C. Lloyd, E. Brunk, N. Mih, A. Sastry, Z. King, R. Takeuchi, W. Nomura, Z. Zhang, H. Mori, A. Feist, and B. Palsson, "iML1515, a knowledgebase that computes *Escherichia coli* traits," Nat. Biotechnol., vol. 35, no. 10, pp. 904–8, 2017.

[40] R. Schuetz, N. Zamboni, M. Zampieri, M. Heinemann, and U. Sauer, "Multidimensional optimality of microbial metabolism," Science, vol. 336, no. 6081, pp. 601–4, 2012.

[41] K. Andersen and K. von Meyenburg, "Are growth rates of escherichia coli in batch cultures limited by respiration?," J. Bacteriol., vol. 144, no. 1, pp. 114–123, 1980.

[42] H. Kubitschek, W. Baldwin, S. Schroeter, and R. Graetzer, "Independence of buoyant cell density and growth rate in *Escherichia coli*," J. Bacteriol., vol. 158, no. 1, pp. 296–99, 1984.

[43] M. Basan, M. Zhu, X. Dai, M. Warren, D. Sévin, Y.-P. Wang, and T. Hwa, "Inflating bacterial cells by increased protein synthesis," Mol. Syst. Biol., vol. 11, no. 10, p. 836, 2015.

[44] A. Wolfe, "The acetate switch," Microbiol. Mol. Biol. Rev., vol. 69, no. 1, pp. 12–50, 2005.

[45] B. Enjalbert, F. Letisse, and J. Portais, "Physiological and molecular timing of the glucose to acetate transition in *Escherichia coli*," Metabolites, vol. 3, no. 3, pp. 820–37, 2013.

[46] H. Waegeman, J. Beauprez, H. Moens, J. Maertens, M. D. Mey, M. Foulquié-Moreno, J. Heijnen, D. Charlier, and W. Soetaert, "Effect of *iclR* and *arcA* knockouts on biomass formation and metabolic fluxes in *Escherichia coli* K12 and its implications on understanding the metabolism of *Escherichia coli* BL21 (DE3)," BMC Microbiol., vol. 11, p. 70, 2011.

[47] C. Long, J. Gonzalez, A. Feist, B. Palsson, and M. R. Antoniewicz, "Fast growth phenotype of *E. coli* K-12 from adaptive laboratory evolution does not require intracellular flux rewiring," Metab. Eng., vol. 44, pp. 100–7, 2017.

[48] C. Cheng, E. O'Brien, D. McCloskey, J. Utrilla, C. Olson, R. LaCroix, T. Sandberg, A. Feist, B. Palsson, and Z. King, "Laboratory evolution reveals a two-dimensional rate-yield tradeoff in microbial metabolism," PLoS Comput. Biol., vol. 15, no. 6, p. e1007066, 2019.

[49] D. Davidi and R. Milo, "Lessons on enzyme kinetics from quantitative proteomics," Curr. Opin. Biotechnol., vol. 46, pp. 81–9, 2017.

[50] S. Donati, T. Sander, and H. Link, "Crosstalk between transcription and metabolism: how much enzyme is enough for a cell?," Wiley Interdiscip. Rev. Syst. Biol. Med., vol. 10, no. 1, p. e1396, 2018.

[51] K.-K. Cheng, B.-S. Lee, T. Masuda, T. Ito, K. Ikeda, A. Hirayama, L. Deng, J. Dong, K. Shimizu, T. Soga, M. Tomita, B. Palsson, and M. Robert, "Global metabolic network reorganization by adaptive mutations allows fast growth of *Escherichia coli* on glycerol," Nat. Commun., vol. 5, p. 3233, 2014.

[52] R. Adadi, B. Volkmer, R. Milo, M. Heinemann, and T. Shlomi, "Prediction of microbial growth rate versus biomass yield by a metabolic network with kinetic parameters," PLoS Comput. Biol., vol. 8, no. 7, p. e1002575, 2012.

[53] M. Wortel, E. Noor, M. Ferris, F. Bruggeman, and W. Liebermeister, "Metabolic enzyme cost explains variable trade-offs between microbial growth rate and yield," PLoS Comput. Biol., vol. 14, no. 2, p. e1006010, 2018.

[54] Q. Beg, A. Vazquez, J. Ernst, M. de Menezes, Z. Bar-Joseph, A.-L. Barabási, and Z. Oltvai, "Intracellular crowding defines the mode and sequence of substrate uptake by *Escherichia coli* and constrains its metabolic activity," Proc. Natl Acad. Sci. USA, vol. 104, no. 31, pp. 12663–68, 2007.

[55] K. Zhuang, G. Vemuri, and R. Mahadevan, "Economics of membrane occupancy and respiro-fermentation," Mol. Syst. Biol., vol. 7, p. 500, 2011.

[56] M. Szenk, K. Dill, and A. de Graff, "Why do fast-growing bacteria enter overflow metabolism? testing the membrane real estate hypothesis," Cell Syst., vol. 5, no. 2, pp. 95–104, 2017.

[57] S. Hui, J. Silverman, S. Chen, D. Erickson, M. Basan, J. Wang, T. Hwa, and J. Williamson, "Quantitative proteomic analysis reveals a simple strategy of global resource allocation in bacteria," Molecular Systems Biology, vol. 11, no. 1, p. 784, 2015.

[58] V. Chubukov, L. Gerosa, K. Kochanowski, and U. Sauer, "Coordination of microbial metabolism," Nat. Rev. Microbiol., vol. 12, no. 5, pp. 327–40, 2014.

[59] D. Erickson, S. Schink, V. Patsalo, J. Williamson, U. Gerland, and T. Hwa, "A global resource allocation strategy governs growth transition kinetics of *Escherichia coli*," Nature, vol. 551, no. 7678, pp. 119–23, 2017.

[60] P. Millard, K. Smallbone, and P. Mendes, "Metabolic regulation is sufficient for global and robust coordination of glucose uptake, catabolism, energy production and growth in *Escherichia coli*," PLoS Comput. Biol., vol. 13, no. 2, p. e1005396, 2017.

[61] T. Pfeiffer, S. Schuster, and S. Bonhoeffer, "Cooperation and competition in the evolution of ATP-producing pathways," Science, vol. 292, no. 5516, pp. 504–7, 2001.

[62] S. Fendt, J. Buescher, F. Rudroff, P. Picotti, M. Zamboni, and U. Sauer, "Tradeoff between enzyme and metabolite efficiency maintains metabolic homeostasis upon perturbations in enzyme capacity," Mol. Syst. Biol., vol. 6, p. 356, 2010.

[63] H. Dourado, M. Mori, T. Hwa, and M. Lercher, "On the optimality of the enzyme-substrate relationship in bacteria," PLoS Biol., vol. 19, no. 10, p. e3001416, 2021.

[64] J. van Elsas, A. Semenov, R. Costa, and J. Trevors, "Survival of *Escherichia coli* in the environment: fundamental and public health aspects," ISME J., vol. 5, no. 2, pp. 173–183, 2011.

[65] G. Valentini, L. Chiarelli, R. Fortin, M. Speranza, A. Galizzi, and A. Mattevi, "The allosteric regulation of pyruvate kinase," J. Biol. Chem., vol. 275, no. 24, pp. 18145–52, 2000.

[66] K. Kochanowski, B. Volkmer, L. Gerosa, B. H. van Rijsewijk, A. Schmidt, and M. Heinemann, "Functioning of a metabolic flux sensor in *Escherichia coli*," Proc. Natl. Acad. Sci. USA, vol. 110, no. 3, pp. 1130–5, 2013.

[67] A. Kremling, K. Bettenbrock, and E. Gilles, "Analysis of global control of *Escherichia coli* carbohydrate uptake," BMC Syst. Biol., vol. 1, no. 1, p. 42, 2007.

[68] I. Yegorov, F. Mairet, H. de Jong, and J.-L. Gouzé, "Optimal control of bacterial growth for the maximization of metabolite production," J. Math. Biol., vol. 78, no. 4, pp. 985–1032, 2019.